



Small-sized long wavelength infrared absorber with perfect ultra-broadband absorptivity

YU ZHOU,^{1,2}  ZHONGZHU LIANG,^{1,*} ZHENG QIN,^{1,2} ENZHU HOU,^{1,2} XIAOYAN SHI,^{1,2} YUHAO ZHANG,^{1,2} YING XIONG,^{1,2} YINHUI TANG,^{1,2} YANDONG FAN,^{1,2} FUMING YANG,^{1,2} JINGQIU LIANG,¹ CHANGHONG CHEN,³ AND JIANJUN LAI³

¹State Key Laboratory of Applied Optics, Changchun Institute of Optics, Fine Mechanics and Physics, Chinese Academy of Sciences, Changchun, Jilin, 130033, China

²University of the Chinese Academy of Sciences, China

³Wuhan National Laboratory for Optoelectronics, Huazhong University of Science and Technology, Wuhan 430074, China

*liangzz@ciomp.ac.cn

Abstract: Two types of ultra-broadband long wavelength infrared (LWIR) absorbers with small period and super thin thickness are designed. The absorption with high absorptivity and large bandwidth is achieved through combined propagating and localized surfaced plasmon resonances. We first design a three-layer absorber with a Ti-Ge-Ti configuration, the period of the structure is only 1.4 μm (nearly 1/8 of the center wavelength), the thickness of its dielectric is only 0.5 μm (1/22 of the center wavelength), and the average absorption is 87.9% under normal incident from 8 μm to 14 μm . Furthermore, the four-layer absorber with a Ti-Ge-Si₃N₄-Ti configuration is designed to obtain more average absorption increasing to 94.5% from 8 μm to 14 μm under normal incident, the period of the structure increases to 1.6 μm and the total thickness of dielectric increases to 0.6 μm . The proposed absorber is polarization-independent and possesses a good tolerance of incident angle. We calculate that the average absorption of the four-layer absorber for both TE- and TM-modes still exceeds 90% up to an incident angle of $\theta = 40^\circ$ (90.7% for TE-mode, 91.9% for TM-mode), and exceed 80% up to an incident angle of $\theta = 60^\circ$ (80.2% for TE-mode, 82.1% for TM-mode).

© 2020 Optical Society of America under the terms of the [OSA Open Access Publishing Agreement](#)

1. Introduction

Metamaterial perfect absorbers (MPAs) can achieve unity absorptivity of corresponding electromagnetic waves, and show excellent performance in many scientific and technical applications due to their perfect absorption and subwavelength thickness [1–4]. The initial structure usually consists of a top metal layer of periodic micro/nano-structures of electric resonators, a continuous middle dielectric or insulator spacer layer, and a bottom metal layer of cut wire or a ground plane to act as a perfect reflector. Since Landy *et al.* experimentally demonstrated the first microwave metamaterial perfect absorber of a periodic Cu-FR4-Cu three-layer structure [5], research into metamaterial absorbers has accelerated. Until now, metamaterial absorbers have extended from visible to near infrared (NIR) [2,6–14], mid-infrared (MIR) [15–18], and long wavelength infrared (LWIR) [19–23] and THz [24–28] regions.

The absorption bandwidth is one of the most important metrics for applications of an absorber. Traditional way to expand the absorption band is to use a multi-sized microstructure to obtain different resonant wavelengths, and then to adjust the size of the microstructures to couple their resonances for a large absorption bandwidth [17–21]. The absorption mechanism of absorbers with multiple resonators is that they couple only various localized surface plasmon modes to achieve large bandwidth and high absorptivity, and discard absorption characteristics dominated by the propagating surface plasmon resonance. Multi-sized structures make the unit

cell large and complicated, difficult to fabricate, and intolerant of polarization and incident angle. Designing a small-sized absorber is a new breakthrough. For instance, absorbers integrated onto the small pixels of the uncooled infrared detector need high and broadband absorption, ultrathin thickness, and simple structure [29]. An absorber with a thick dielectric can obtain good absorptivity but increases thermal capacity, and greater thermal capacity implies more noise equivalent temperature difference (NETD). An ultrathin broadband absorber is also required for many applications, such as thermal emitters [30], photovoltaics (PV) [31], imaging [32], and micro-lenses [33].

In this paper, we design two types of ultra-broadband absorbers that can achieve high absorptivity and broad bandwidth of the LWIR spectrum; one is a three-layer structure based on an initial metal–insulator–metal (MIM) configuration, whereas the other uses two layers of different materials (Ge and Si₃N₄), with the top and bottom metal layers consisting of a four-layer structure. Titanium is used for the top and bottom layers of the absorbers due to its high-loss characteristics. The top layer consists of a central nano–ring and four symmetric nano–antenna resonators such that the structure possesses good tolerance of polarization angles, and the bottom and dielectric layers are continuous planar films. Three-dimensional finite–difference time–domain simulations were performed to calculate the absorption spectrum of the designed absorbers. The average absorption of the three-layer structure is 87.9% from 8μm to 14μm and increases to 94.5% for the four-layer structure. We calculate the average absorptions of the four-layer absorber at the incident angle of ± 60° for TE–mode and TM–mode are 80.2% and 82.1%.

2. Design of ultra-broadband absorber of three-layer structure

Surface plasmons (SPs) are waves that propagate along the surface of a conductor, usually a metal [34], they are usually divided into two categories: localized surface plasmons (LSPs) and propagating surface plasmons (PSPs). The collectively resonant oscillations of electrons on the surface of metal particles excited by an electric field of incident light is called localized surface plasmon resonance (LSPR), and the PSPs are evanescent waves that propagate along the interface between the conductor and dielectric. Unlike with LSPs, a specially nonlocalized mode is produced by metal surface electrons under the excitation of incident light. To simply illustrate the effects of the absorption dominated by the propagating surface plasmon (PSP) and localized surface plasmon (LSP) modes, we first investigate the structure of a unit cell with a Ti nano–disk and a nano–ring placed at the top of the dielectric layer, as shown in Fig. 1(a)–1(b). The structure is illuminated by a TM–polarized plane wave. The period of the structure is 1.4 μm, the thickness of Ge layer is 0.5 μm, and the thickness of nano–disk or nano–ring is 20 nm. The thickness (100 nm) of the substrate (Ti) prevents light being transmitted through the structure. The unit cell consists of three layers (Ti–Ge–Ti) based on a metal–insulator–metal (MIM) structure. We choose titanium (Ti) because it is one of the best metals with lossy characteristics in the infrared region and Germanium (Ge), which is almost lossless and has a nearly constant refractive index of 4 in the LWIR band and is a suitable candidate for the dielectric due to its high refractive index. In our designed absorber, PSPs resonance wavelengths are determined by the following equation:

$$k = k_0 \sin \theta \pm i2\pi/L \quad (1)$$

$$k_{PSP} = k_0[\varepsilon_m \varepsilon_d / \varepsilon_m + \varepsilon_d]^{1/2} \quad (2)$$

Equation (1) is the Bragg coupling condition, where $k_0 = \omega/c$ is the free space wavevector, θ is the incident angle, i is an integer, represents the order of grating, L is the grating period. Equation (2) indicates the wavevector of PSPs, ε_m and ε_d are the dielectric constant of top metal and middle dielectric layer [35]. For the MIM absorber, PSPs are excited by top metal structure and propagating at the interface, when $k = k_{PSP}$ does the incident wave couple to PSPs. For LSPs

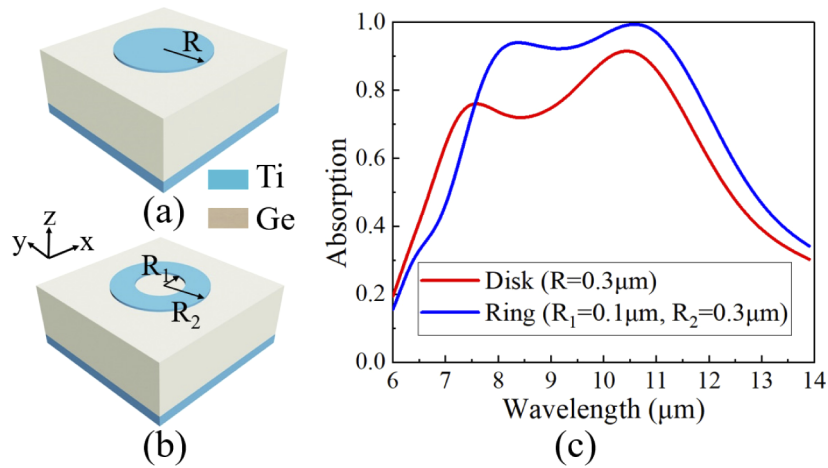


Fig. 1. (a) Nano-disk at the top of insulator of unit cell. (b) Nano-ring at the top of insulator of unit cell. (c) Absorption spectrum of different upper Ti metal structures.

resonances in upper nano-disk and nano-ring structures, an empirical formula can be expressed the resonance frequency or wavelength [24]:

$$2\pi r = c / (f \sqrt{\epsilon_{eff}}) = \lambda / \sqrt{\epsilon_{eff}} \quad (3)$$

Where $r = (R_1 + R_2)/2$ is the average radius of the upper nano-ring structure, c is the speed of light in free space, and disk can be imaged as a ring with $R_1 = 0$, so $r = R$ for upper nano-disk structure. ϵ_{eff} is the effective dielectric constant of the dielectric layer, ϵ_{eff} is sensitive to thickness and the period of the structure. The absorption spectrum of the absorber with different top structures at normal incidence is shown in Fig. 1(c). Both of the upper nano-disk and nano-ring structure can produce two absorption peaks which are dominated by PSPs and LSPs resonances, respectively. For the upper nano-disk structure, two absorption peaks are located at 7.60 μm and 10.42 μm , with absorptivity of 76.01% and 91.50%; and for upper nano-ring structure, two absorption peaks are located at 8.40 μm and 10.59 μm with absorptivity of 94.01% and 99.41%.

The electromagnetic field distributions of the upper nano-disk structure and the upper nano-ring structure at each resonant wavelength are investigated, as shown in Fig. 2. It can be seen from Fig. 2(a)–2(d) that the electric field is strongly confined mainly in the air-slot of the upper Ti structure, implying that the surface plasmon polaritons (SPPs) are excited in the metamaterial absorber. Two different resonant modes are observed in Fig. 2(e)–2(h). At the wavelength of their first absorption peaks, the PSP mode dominates absorption, as shown in Fig. 2(e) and 2(g); and the LSP mode dominates absorption at their second peaks, as shown in Fig. 2(f) and 2(h). The difference between upper nano-disk structure and the upper nano-ring structure is that surface plasmons can be generated on the inner surface of the nano-ring. It can excite a different surface plasmon mode compared to the upper nano-disk structure. For the ring resonators, the direction of the surface current and electric field of the inner and the outer surfaces are reversed, leading to counteracting resonances on the inner and outer surfaces [36]. It can be found that at the PSPs-dominated absorption peak of the upper nano-disk or nano-ring structure, there is also low-intensity LSPs resonance excited by upper metallic structure, as shown in Fig. 2(e) and 2(g), the PSPs resonance excited by nano-ring is stronger than nano-disk, implying that the low-intensity LSPs resonance affects the PSPs resonance, leading to low absorption enhancement. The counteracting resonance excited by inner surface of nano-ring gradually reduces as the wavelength increases, then upper nano-ring structure can also excite stronger LSPs resonance to enhance the absorption because surface plasmons can hardly generate at the inner surface as the

wavelength gradually increasing. To couple PSP and LSP resonances to expand the bandwidth and increase absorption, the upper nano-ring structure with suitable sizes can achieve more desirable absorptivity and bandwidth than the upper nano-disk structure.

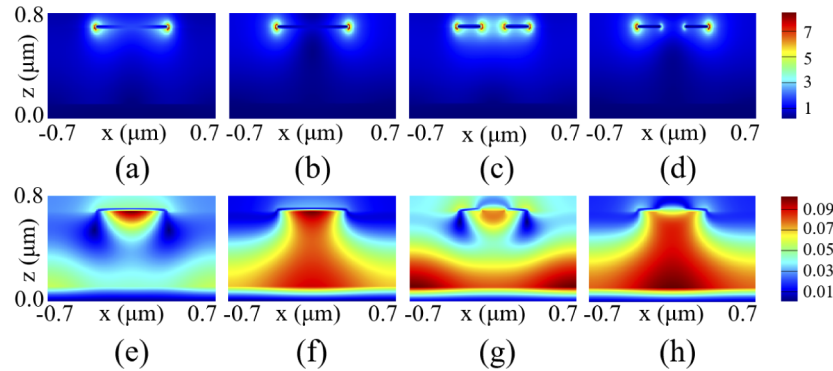


Fig. 2. (a)–(b) Electric field distributions of the upper nano-disk structure at the wavelength of 7.60 μm and 10.42 μm . (c)–(d) Electric field distributions of the upper nano-ring structure at the wavelength of 8.40 μm and 10.59 μm . (e)–(f) Magnetic field distributions of the upper nano-disk structure at the wavelength of 7.60 μm and 10.42 μm . (g)–(h) Magnetic field distributions of the upper nano-ring structure at the wavelength of 8.40 μm and 10.59 μm . (colored bars in x – z plane, $y = 0$)

The PSP-dominated and LSP-dominated absorption peaks can be tuned by changing the radius of the nano-disk and the nano-ring, as shown in Fig. 3(a), it indicates that the LSPs resonance is more dependent on sizes of top metal structure than PSPs, in fact, nearly all parameters in the absorber affect the LSPs resonance. And PSPs resonance, by contrast, is mainly depended on the effective dielectric constant of top metal layer and middle dielectric layer, small changes of sizes of top metal structures nearly do not affect the effective dielectric constant of top metal layer. However, the wavelengths of two absorption peaks of every structure from Fig. 3(a) cannot represent PSPs and LSPs real resonances wavelengths, because at each absorption peak, there is also low-intensity PSPs or LSPs resonance affect the absorption that make the peaks shift from the calculated resonance wavelengths of LSPs or PSPs. Moreover, it can be concluded from Eq. (3) that the wavelength of LSPs resonances excited by nano-ring structure are not affected by permittivity of top metal, so we simulate the absorption used Au for metallic nano-ring, as shown in Fig. 3(b). It is observed that the wavelength of LSP-dominated absorption peak by Au is nearly the same as Ti. It is calculated that the Au nano-ring structure has an LSPs-dominated absorption peak at wavelength of 10.25 μm with the absorptivity of 68.78%. The permittivity of Au is much higher than Ti, so upper Au nano-ring structure is harder to excite PSPs resonance than upper Ti nano-ring structure, the difference of 0.17 μm between two LSPs-dominated absorption peaks are caused by low-intensity PSP resonance. In some studies, traditional noble metals such as Au [20,21] and Ag [19] are also usually used to realize broadband absorption, the parameters of these absorbers with multi-sized resonant structures can be near-perfectly calculated such as building an equivalent *PLC* circuit model [19] because low-intensity PSPs resonances which are excited by noble metals have little or no effects on absorption characteristics. Noble metals also have advantages that absorption dominated by LSP resonances can be flexibly controlled and easily coupled for broadband absorption such as using a metasurface with many Au particles [7], it does not need to consider the negative effect which is produced by low-intensity PSPs resonance then reduce the LSP resonances. However, in order to design easy, periodic and symmetric structures, refractory metals, such as Ti [11,14,22] and Ni [23] which have highly lossy characteristics

and produce low- Q resonances, are used to achieve perfect ultra-broadband absorption, and refractory metals are also more stable for irradiation and high temperature than noble metals.

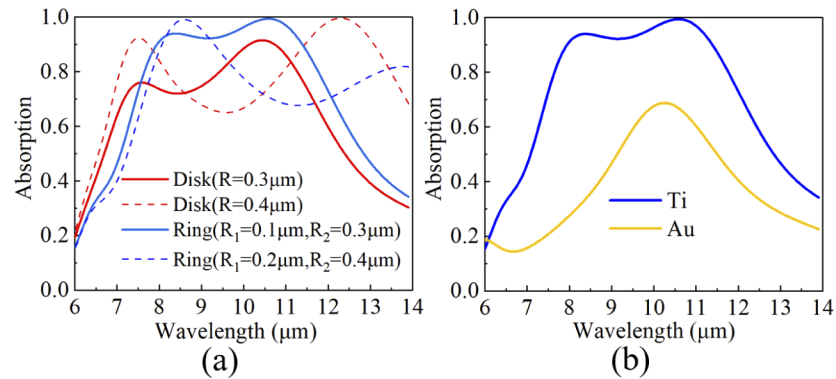


Fig. 3. (a) Absorption spectrum with different R , R_1 and R_2 . (b) Absorption spectrum with different top metals of Ti and Au.

Then we design the structure of the previous nano-ring unit cell with four nano-antennas at the top of the Ge layer; the nano-antennas are located at the border of the unit cell, as shown in Fig. 4(a)–(b). The thickness of the titanium bottom (h_1) is 100 nm, which is sufficient to inhibit any incident light transmitted through the multilayer structure, leading to nearly zero transmission in the LWIR band. The thickness of the germanium dielectric (h_2) is $0.5\mu\text{m}$, and the thickness of the metal top of titanium (h_3) is 20 nm. A thinner titanium metal layer promises a less lossy cavity and guarantees sufficient coupling effects. The period (p) of the structure is only $1.4\mu\text{m}$. The length (s) and width (b) of the nano-antennas are $0.8\mu\text{m}$ and $0.1\mu\text{m}$, respectively, and the inner and outer radius of nano-rings R_1 and R_2 are $0.1\mu\text{m}$ and $0.3\mu\text{m}$, respectively. In Fig. 4(c), the blue curve shows the absorptivity of the proposed absorber with the whole Ti–Ge–Ti structure. The absorption curve from $8\mu\text{m}$ to $14\mu\text{m}$ exceeds 85% at all times, and the average absorption in the LWIR band is calculated as 87.9%. The absorption spectrum is shown as Fig. 4(c), it is calculated that three peaks of $8.15\mu\text{m}$, $10.77\mu\text{m}$ and $13.14\mu\text{m}$ with absorptivity of 94.03%, 93.23% and 88.85% are coupling to the broad bandwidth. It is easy to verify that PSPs resonances dominate the peak of $8.15\mu\text{m}$, and LSPs resonances dominate the peaks of $10.77\mu\text{m}$ and $13.14\mu\text{m}$. The purple and red dashed curves show the absorptivity of the structure with only nano-ring and nano-antennas on the top, and comparison of the results shows that the ultra-broadband absorption spectra are the superposition of the LSP resonances of different upper metal structures.

Figure 5 shows the magnetic field distributions of three absorption peaks. The absorption mechanism of coupling nano-ring and nano-antennas LSPs resonances is a bit like the traditional way by coupling multi-sized resonant structures to realize broad bandwidth [17–21]. As the LSPs resonances excited by nano-ring decreasing, the nano-antenna resonances gradually dominate the absorption and then the absorber can achieve a broader bandwidth compared to previous upper nano-ring structure.

We further examined the influence on absorption of a change of length (s) and width (b) of the nano-antenna, as shown in Fig. 6(a) and 6(b). It is seen that the absorption property of the proposed absorber is sensitive to the parameters s and b , but the absorber can achieve >85% of the average absorption with the parameters s and b from 700–800 nm and 80–120 nm, respectively. The LSPs-dominated absorption can be tuned by the s and b parameters. The nano-antennas would not affect the position of the PSPs-dominated resonant wavelength, but it would reduce the absorption. The parameter b greatly affects the size of the nano-antennas, and

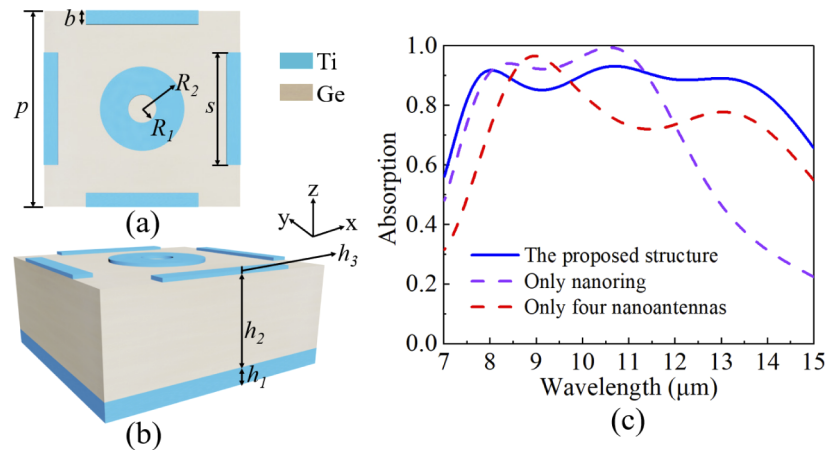


Fig. 4. (a) Top view of unit cell. (b) Lateral view of unit cell. (c) Simulated absorption spectrum of proposed absorber.

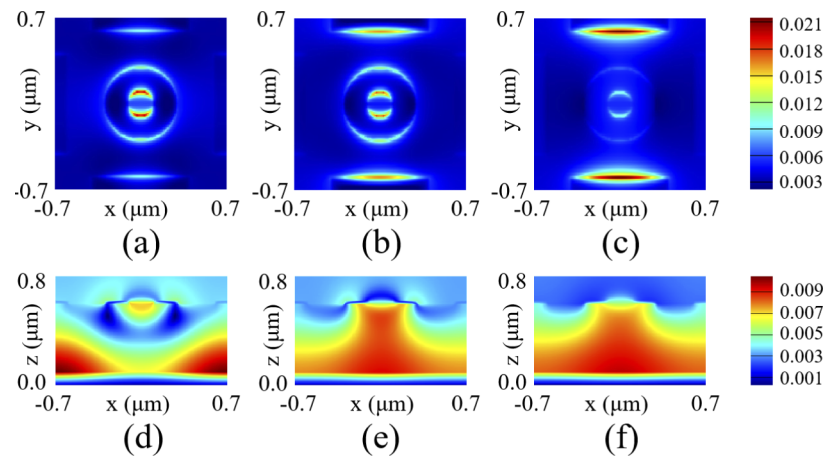


Fig. 5. Magnetic field distributions of top layer at the wavelength of (a) 8.15 μm (b) 10.77 μm and (c) 13.14 μm , respectively (colored bars in x - y plane); Lateral magnetic field distributions of (d) 8.15 μm (e) 10.77 μm and (f) 13.14 μm , respectively (colored bars in x - z plane, $y = 0$). It indicates that the PSPs resonances dominate the absorption peak of 8.15 μm , then superposed LSPs resonances excited by nano-ring and nano-antennas dominate the absorption peaks of 10.77 μm and 13.14 μm . (The structure is illuminated by a TM-polarized plane wave.)

the PSPs-dominated absorption is inversely proportional to the size of the nano-antennas. In fact, the PSPs are generated on the interface between the bottom Ti film and the dielectric, and is dependent less on the metal structure in the top of absorber, whereas the top metal structure covering on the dielectric, especially at the borders, reduces incident radiation interactions on the structure to generate propagating surface plasmons, decreasing the intensity of the PSP mode. The advantage of putting nano-antennas at the border of structure is that this method not only expands the bandwidth, but also reduces the total amount of metal structure and difficulties of fabrication. The absorptivity and absorption bandwidth are related to the effective dielectric constant [37]. For metamaterials, the effective dielectric constant is related to the components and sizes (period, thickness), and the choice of material and design sizes all affect the absorption

characteristics [38]. The PSPs and LSPs resonances are sensitive to the thickness and period. Figure 6(c) shows that the thickness of the dielectric greatly affects the absorption characteristics: as the thickness of the dielectric increases, the effective dielectric constant of the dielectric becomes larger, leading to an increase in resonant wavelength. Figure 6(d) shows that the period of the structure also affects the absorption bandwidth and PSPs-dominated resonance wavelength and absorptivity. The absorption bandwidth decreases at the same time as the average absorption increases before the second LSPs-dominated peak, along with the increasing period of the absorber.

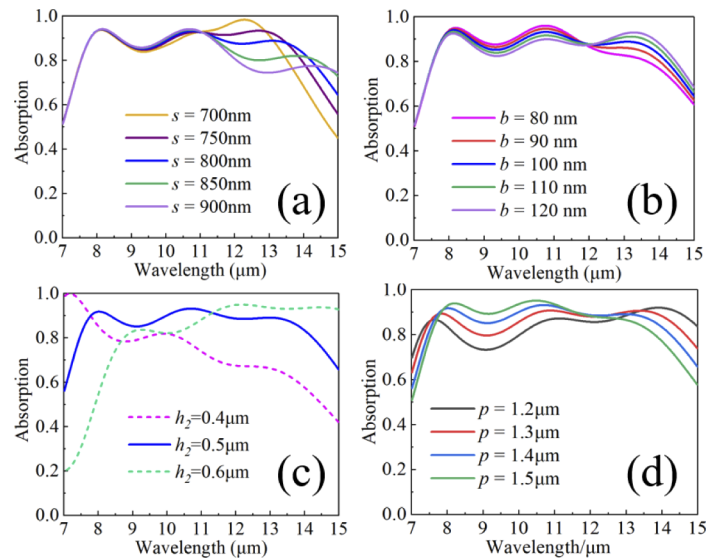


Fig. 6. (a) Absorption spectrum with different length (s) of nano-antennas. (b) Absorption spectrum with different width (b) of nano-antennas. (c) Absorption spectrum with different thickness of middle dielectric (h_2). (d) Absorption spectrum with different period (c).

3. High-absorptivity absorber with multi-layer dielectric

The proposed four-layer absorber is shown in Fig. 7(a)–7(c). The top and bottom metal structures use by titanium, as in previous structure. The middle dielectric consists of two different materials: germanium (Ge) and silicon nitride (Si_3N_4). The period (p) of the absorber is $1.6\mu\text{m}$ ($0.2\mu\text{m}$ larger than previous structure), and the total thickness of dielectric (t_2+t_3) is $0.6\mu\text{m}$ ($0.1\mu\text{m}$ thicker than previous structure). In our experiment, $t_1 = 100\text{ nm}$, $t_2 = 330\text{ nm}$, $t_3 = 270\text{ nm}$, $t_4 = 20\text{ nm}$, $s = 750\text{ nm}$, $b = 100\text{ nm}$, $R_1 = 120\text{ nm}$ and $R_2 = 300\text{ nm}$. The absorption spectrum of the absorber is shown in Fig. 8(a). It is observed from the spectrum that the absorber exhibits high absorption over 90% in a broad wavelength spread from $8.0\mu\text{m}$ to $14.0\mu\text{m}$, which it covers the entire LWIR band. The average absorbance from $8.0\mu\text{m}$ to $14.0\mu\text{m}$ is calculated as 94.5%. The four-layer absorber with optimal size possesses stronger absorption abilities than the previous three-layer absorber, as shown in Fig. 8(b). The three absorption peaks are located at $8.51\mu\text{m}$, $10.47\mu\text{m}$, and $13.05\mu\text{m}$, with the absorptivity of 97.51%, 95.07%, 95.54%, respectively.

The electric and the magnetic field distributions at each resonance wavelength are shown in Fig. 9(a)–9(f). It can be concluded that at the peak of $8.51\mu\text{m}$, the PSPs resonance dominates the absorption, as the wavelength increasing, the LSPs resonances excited by nano-ring and nano-antennas gradually dominate the absorption. Generally, electric field distributions would not generate in a dielectric, but in our structure one can see faint electric field distributions in

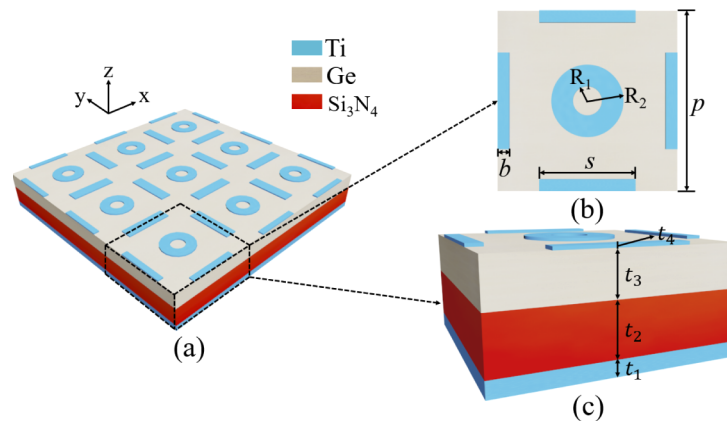


Fig. 7. (a) Schematic diagram of the proposed absorber. (b) Top view of the unit cell of the absorber. (c) Lateral view of the unit cell of the absorber.

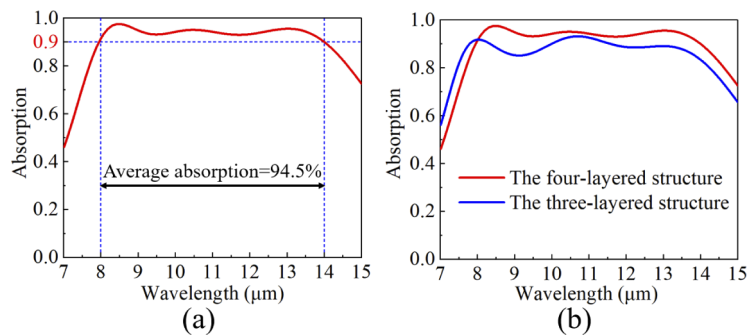


Fig. 8. (a) Absorption spectrum of the four-layer absorber. (b) The comparison of the absorption of the four-layer absorber and the previous three-layer absorber.

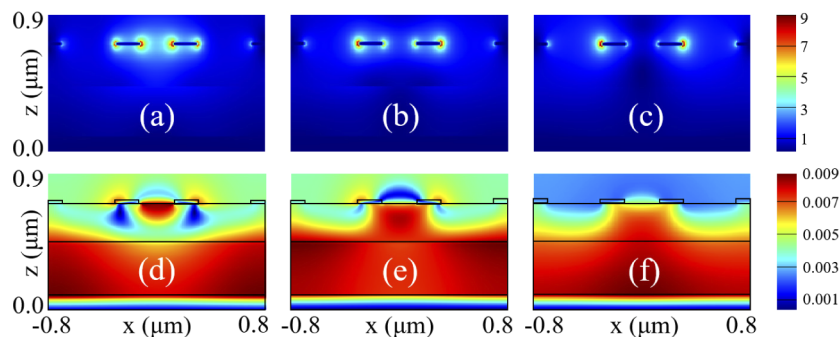


Fig. 9. (a)–(c) Electric field distributions at resonance wavelengths 8.51 μm , 10.47 μm , and 13.05 μm (colored bar in x - z plane, $y = 0$); (d)–(f) Magnetic field distributions at resonance wavelengths 8.51 μm , 10.47 μm , and 13.05 μm (colored bar in x - z plane, $y = 0$).

the Si_3N_4 layer, which gradually disappears as the PSPs resonance vanishes. Silicon nitride is a distinctive dielectric material that can generate electric fields slightly when the incident plane wave shoots onto the structure that enhance the PSPs resonance, leading to increased first absorption peak, as shown in Fig. 10(a). A larger proportion of Si_3N_4 layer leads to a broader

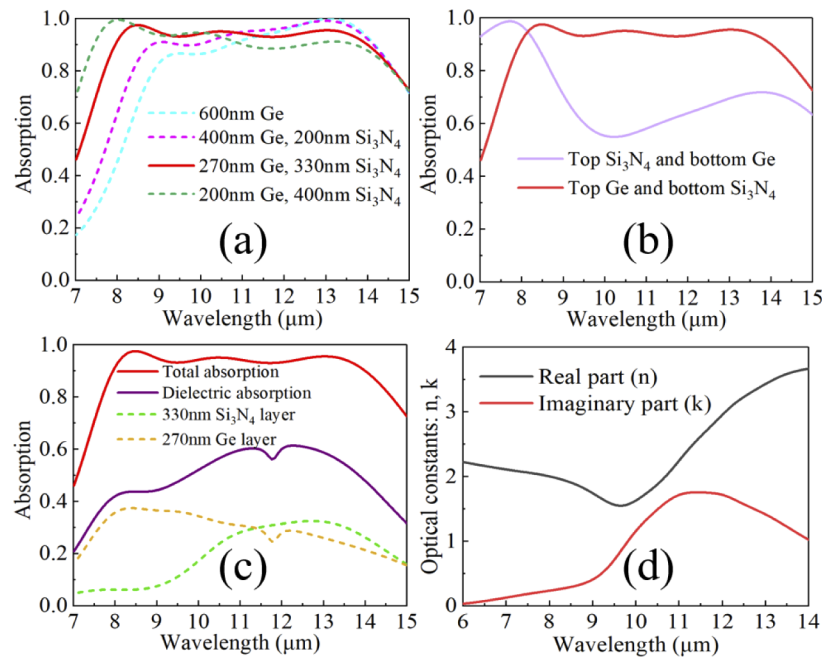


Fig. 10. (a) Absorption spectrum of different proportions of Si₃N₄ and Ge in the dielectric. (b) Absorption spectrum of changing the positions of the Ge and Si₃N₄ layers. (The total thickness of the dielectric is 0.6 μm). (c) Absorption contributions from each dielectric layer for four-layered Ti-Ge-Si₃N₄-Ti absorber. (d) Real and Imaginary part of refractive index of Si₃N₄ thin film.

bandwidth, but gradually reduces the third absorption peak. Figure 10(b) shows that changing the position of the two different dielectric layers leads to greater changes in the absorption spectrum, which indicates that placing the Si₃N₄ layer at the top of dielectric leads to energy leakage. It is much better to place the Ge layer at the top and the Si₃N₄ layer at the bottom, as optimizing the thickness of the two layers can achieve high average absorptivity and greater bandwidth. The intrinsic absorption of dielectric layers for the four-layered Ti-Ge-Si₃N₄-Ti absorber is calculated in Fig. 10(c), and Fig. 10(d) shows the optical constants of Si₃N₄ layer. It can be observed that Si₃N₄ has a unique imaginary part of refractive index in LWIR regime that can increase intrinsic absorption from 8–14 μm. Previous study shows that increasing the thickness of the Ge layer makes a redshift for absorption bandwidth. And dielectric layer with larger refractive index can also makes a redshift for intrinsic absorption bandwidth [37]. Giving the Si₃N₄ layer a lower refractive index than Ge in the dielectric decreases the effective refractive index of total dielectric, making the absorption bandwidth shift to the left in order to locate it at suitable places. The absorber with such a laminated dielectric can achieve excellent absorption bandwidth that single dielectric hardly realizes.

Finally, spectrum of absorptions with oblique incidences for both TE-polarized ($\varphi = 0^\circ$) and TM-polarized ($\varphi = 90^\circ$) waves are shown in Fig. 11(a) and 11(b), respectively. At small incident angles, one can see that the proposed absorber shows almost angle-independent absorption for both the TE- and TM-modes due to its small size and symmetric resonators, and the absorption spectrum is almost unchanged for both polarizations with incident angles up to 20° . We calculate that the average absorption for the TE- and TM-modes from 8 μm to 14 μm are 90.7% and 91.9%, respectively, at the angle of incidence $\theta = 40^\circ$. They are 80.2% and 82.1%, respectively, and at the angle of incidence $\theta = 60^\circ$. For large incident angles, the absorber behaves differently for TE-

and TM-polarized waves. As the incident angle increases, average absorptivity and bandwidth gradually decrease with fluctuations. The horizontal component of the incident magnetic field decreases as the incident angle increases, and the strength of the coupling and the absorption weakens. Comparing other LWIR broadband absorbers with large and complicated structures, our absorber can achieve excellent wide-angle performance.

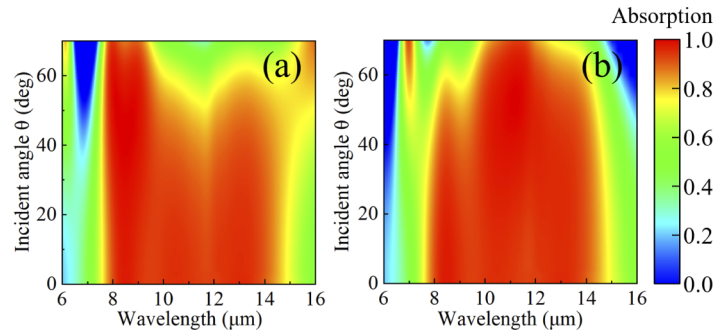


Fig. 11. Absorption spectra with different incident angles for (a) TE-mode (x-polarized) and (b) TM-mode (y-polarized).

4. Conclusion

In summary, the three-layer (Ti-Ge-Ti) and the four-layer (Ti-Ge-Si₃N₄-Ti) absorbers were designed and succeeded in coupling propagating and localized surface plasmon resonances to achieve an absorption spectrum with high absorptivity and large bandwidth. The absorption dominated by the PSP and LSP resonances can be tuned flexibly by changing the various parameters of the structure. The effects of the upper nano-disk and nano-ring structures, different sizes of resonators, and different parameters of dielectric layers on absorption performance are compared in detail to investigate the characteristics of the three- and four-layer absorbers. The proposed absorbers have a super-thin structure, as well as ultra-broadband absorption. The average absorption from 8 μm to 14 μm of the three- and four-layer absorbers are 87.9% and 94.5%, respectively, with the total thicknesses of 0.62 μm and 0.72 μm , respectively. For designing the four-layer absorber, the red shift of absorption spectrum caused by increasing thickness of dielectric can be eliminated by inserting Si₃N₄ which can also excite PSP-dominated absorption, leads to more absorptivity and larger bandwidth. The average absorption of the four-layer absorber for both TE- and TM-modes still exceeds 90% up to an incident angle of $\theta = 40^\circ$ (90.7% for TE-mode, 91.9% for TM-mode), and exceed 80% up to an incident angle of $\theta = 60^\circ$ (80.2% for TE-mode, 82.1% for TM-mode). The proposed ultra-broadband metamaterial absorbers show promise in applications such as thermal emitters and infrared imaging, and for integrating into small-pixel uncooled infrared detectors.

Funding

National Natural Science Foundation of China (61735018, 61376122, 61805242); Scientific and Technological Development Project of Jilin Province (20170204077GX, 20190103014JH); Excellent Member of Youth Innovation Promotion Association of the Chinese Academy of Sciences (2014193); Leading Talents and Team Project of Scientific and Technological Innovation for Young and Middle-aged Groups in Jilin Province (20190101012JH); Overseas Students Science and Technology Innovation and Entrepreneurship Projects; Project of CIOMP-Duke Collaborative Research; Project of CIOMP-Fudan University Collaborative Research; Independent fund of State Key Laboratory of Applied Optics.

Disclosures

The authors declare no conflicts of interest.

References

1. H. Lin, B. C. P. Strumberg, K. Lin, Y. Yang, X. Zheng, T. K. Chong, C. M. de Sterke, and B. Jia, "A 90-nm-thick graphene metamaterial for strong and extremely broadband absorption of unpolarized light," *Nat. Photonics* **13**(4), 270–276 (2019).
2. N. Liu, M. Mesch, T. Weiss, M. Hentschel, and H. Giessen, "Infrared perfect absorber and its application as Plasmonic Sensor," *Nano Lett.* **10**(7), 2342–2348 (2010).
3. T. D. Dao, K. Chen, S. Ishii, A. Ohi, T. Nabatame, M. Kitajima, and T. Nagao, "Infrared perfect absorbers fabricated by colloidal mask etching of Al–Al₂O₃–Al trilayers," *ACS Photonics* **2**(7), 964–970 (2015).
4. L. Feng, P. Huo, Y. Liang, and T. Xu, "Photonic Metamaterial Absorbers: Morphology Engineering and Interdisciplinary Applications," *Adv. Mater.* 1903787 (2019).
5. N. I. Landy, S. Sajuyigbe, J. J. Mock, D. R. Smith, and W. J. Padilla, "Perfect metamaterial absorber," *Phys. Rev. Lett.* **100**(20), 207402 (2008).
6. K. T. Lee, C. Ji, and L. J. Guo, "Wide-angle, polarization-independent ultrathin broadband visible absorbers," *Appl. Phys. Lett.* **108**(3), 031107 (2016).
7. Z. Liu, X. Liu, S. Huang, P. Pan, J. Chen, G. Liu, and G. Gu, "Automatically Acquired Broadband Plasmonic-Metamaterial Black Absorber during the Metallic Film-Formation," *ACS Appl. Mater. Interfaces* **7**(8), 4962–4968 (2015).
8. M. Luo, S. Shen, L. Zhou, S. Wu, Y. Zhou, and L. Chen, "Broadband, wide-angle, and polarization-independent metamaterial absorber for the visible regime," *Opt. Express* **25**(14), 16715–16724 (2017).
9. D. Wu, C. Liu, Y. Liu, L. Yu, Z. Yu, L. Chen, R. Ma, and H. Ye, "Numerical study of an ultra-broadband nearperfect solar absorber in the visible and near-infrared region," *Opt. Lett.* **42**(3), 450–453 (2017).
10. W. Li, U. Guler, N. Kinsey, G. V. Naik, A. Boltasseva, J. Guan, V. M. Shalaev, and A. V. Kildishev, "Refractory plasmonics with titanium nitride: broadband metamaterial absorber," *Adv. Mater.* **26**(47), 7959–7965 (2014).
11. Z. Liu, P. Tang, X. Liu, G. Liu, Y. Wang, and M. Liu, "Truncated titanium/semiconductor cones for wide-band solar absorbers," *Nanotechnology* **30**(30), 305203 (2019).
12. Z. Liu, G. Liu, Z. Huang, X. Liu, and G. Fu, "Ultra-broadband perfect solar absorber by an ultra-thin refractory titanium nitride meta-surface," *Sol. Energy Mater. Sol. Cells* **179**(1), 346–352 (2018).
13. L. Lei, S. Li, H. Huang, K. Tao, and P. Xu, "Ultra-broadband absorber from visible to near-infrared using plasmonic metamaterial," *Opt. Express* **26**(5), 5686–5693 (2018).
14. F. Ding, J. Dai, Y. Chen, J. Zhu, Y. Jin, and S. I. Bozhevolnyi, "Broadband near-infrared metamaterial absorbers utilizing highly lossy metals," *Sci. Rep.* **6**(1), 39445 (2016).
15. R. Mudachathi and T. Tanaka, "3D conical helix metamaterial-based isotropic broadband perfect light absorber," *Opt. Express* **27**(19), 26369–26376 (2019).
16. P. Tang, Z. Liu, Y. Wang, X. Liu, P. Pan, and G. Liu, "Ultrawideband midinfrared refractory absorbers," *Opt. Eng.* **58**(11), 1 (2019).
17. Z. Li, L. Stan, D. A. Czapslewski, X. Yang, and J. Gao, "Wavelength-selective mid-infrared metamaterial absorbers with multiple tungsten cross resonators," *Opt. Express* **26**(5), 5616–5631 (2018).
18. C. Fann, J. Zhang, M. Elkabash, W. R. Donaldson, E. M. Campbell, and C. Guo, "Broadband infrared plasmonic metamaterial absorber with multipronged absorption mechanisms," *Opt. Express* **27**(20), 27917–27925 (2019).
19. R. Feng, J. Qiu, L. Liu, W. Ding, and L. Chen, "Parallel LC circuit model for multi-band absorption and preliminary design of radiative cooling," *Opt. Express* **22**(S7), A1713–A1724 (2014).
20. W. Guo, Y. Liu, and T. Han, "Ultra-broadband infrared metasurface absorber," *Opt. Express* **24**(18), 20586–20592 (2016).
21. Y. Cui, J. Xu, K. H. Fung, Y. Jin, A. Kumar, S. He, and N. X. Fang, "A thin film broadband absorber based on multi-sized nanoantennas," *Appl. Phys. Lett.* **99**(25), 253101 (2011).
22. Y. Luo, Z. Liang, D. Meng, J. Tao, J. Liang, C. Chen, J. Lai, Y. Qin, J. Lv, and Y. Zhang, "Ultra-broadband and high absorbance metamaterial absorber in long wavelength Infrared based on hybridization of embedded cavity modes," *Opt. Commun.* **448**, 1–9 (2019).
23. J. Y. Jung, K. Song, J. H. Choi, J. Lee, D. Choi, J. Jeong, and D. P. Neikirk, "Infrared broadband metasurface absorber for reducing the thermal mass of a microbolometer," *Sci. Rep.* **7**(1), 430 (2017).
24. L. Qi and C. Liu, "Broadband multilayer graphene metamaterial absorbers," *Opt. Mater. Express* **9**(3), 1298–1309 (2019).
25. M. Kenney, J. Grant, and D. R. S. Cumming, "Alignment-insensitive bilayer THz metasurface absorbers exceeding 100% bandwidth," *Opt. Express* **27**(15), 20886–20900 (2019).
26. N. Hu, F. Wu, L. Bian, H. Liu, and P. Liu, "Dual broadband absorber based on graphene metamaterial in the terahertz range," *Opt. Mater. Express* **8**(12), 3899–3909 (2018).
27. X. Huang, F. Yang, B. Gao, Q. Yang, J. Wu, and W. He, "Metamaterial absorber with independently tunable amplitude and frequency in the terahertz regime," *Opt. Express* **27**(18), 25902–25911 (2019).

28. Y. Zhao, B. Wu, B. Huang, and Q. Cheng, "Switchable broadband terahertz absorber/reflector enabled by hybrid graphene-gold metasurface," *Opt. Express* **25**(7), 7161–7169 (2017).
29. J. Y. Suen, K. Fan, J. Montaya, C. Bingham, V. Stenger, S. Sriram, and W. J. Pandilla, "Multifunctional metamaterial pyroelectric infrared detectors," *Optica* **4**(2), 276–279 (2017).
30. P. N. Dyachenko, S. Molesky, A. Yu Petrov, M. Störmer, T. Krekeler, S. Lang, M. Ritter, Z. Jacob, and M. Eich, "Controlling thermal emission with refractory epsilon-near-zero metamaterials via topological transitions," *Nat. Commun.* **7**(1), 11809 (2016).
31. F. Priolo, T. Gregorkiewicz, M. Galli, and T. F. Krauss, "Silicon nanostructures for photonics and photovoltaics," *Nat. Nanotechnol.* **9**(1), 19–32 (2014).
32. J. Li, L. Bao, S. Jiang, Q. Guo, D. Xu, B. Xiong, G. Zhang, and F. Yi, "Inverse design of multifunctional plasmonic metamaterial absorbers for infrared polarimetric imaging," *Opt. Express* **27**(6), 8375–8386 (2019).
33. X. Chen, B. Liu, J. Zhu, M. Gu, H. Chen, J. Liang, L. Chen, and X. Ouyang, "Light extraction enhancement and directional control of scintillator by using microlens arrays," *Opt. Express* **26**(18), 23132–23141 (2018).
34. L. B. William, D. Alain, and W. E. Thomas, "Surface plasmon subwavelength optics," *Nature* **424**(6950), 824–830 (2003).
35. Q. Li, J. Gao, H. Yang, H. Liu, X. Wang, Z. Li, and X. Guo, "Tunable plasmonic absorber based on propagating and localized surface plasmons using Metal-Dielectric-Metal structure," *Plasmonics* **12**(4), 1037–1043 (2017).
36. H. Jayatileka, H. Shoman, L. Chrostowski, and S. Shekhar, "Photoconductive heaters enable control of large-scale silicon photonic ring resonator circuits," *Optica* **6**(1), 84–91 (2019).
37. C. M. Watts, X. Liu, and W. J. Paddila, "Metamaterial Electromagnetic Wave Absorber," *Adv. Opt. Mater.* **24**, OP98–OP120 (2012).
38. P. Yu, L. V. Besteiro, Y. Huang, J. Wu, L. Fu, H. H. Tan, C. Jagadish, G. P. Wiederrecht, A. O. Govorov, and Z. Wang, "Broadband Metamaterial Absorbers," *Adv. Opt. Mater.* 1800995 (2018).